Virtual photon structure functions and the parton content of the electron

Manuel Drees
Physics Department, University of Wisconsin, 1150 University Avenue, Madison, Wisconsin 53706

Rohini M. Godbole
Physics Department, Bombay University, Vidyanagari, Bombay 400098, India
(Received 10 March 1994; revised manuscript received 19 May 1994)

We point out that in processes involving the parton content of the photon the usual effective photon approximation should be modified. The reason is that the parton content of virtual photons is logarithmically suppressed compared to real photons. We describe this suppression using several simple, physically motivated *Ansätze*. Although the parton content of the electron in general no longer factorizes into an electron flux function and a photon structure function, it can still be expressed as a single integral. Numerical examples are given for the e^+e^- collider TRISTAN as well as the ep collider HERA.

PACS number(s): 14.70.Bh, 12.38.Bx, 13.60.−r, 13.65.+i

I. INTRODUCTION

Resolved photon processes [1] are now being studied in some detail at both e^+e^- colliders (KEK TRISTAN [2,3], CERN Large Electron-Position Collider (LEP) [4]), and the DESY ep collider HERA [5,6]. These are processes involving the quark and gluon "content" of the photon [7]. The immediate goal of studying such reactions is to determine the photon structure functions experimentally, i.e., to test which (if any) of the parametrizations that have been proposed [8–12] reproduce the data. Ultimately one hopes to gain new insight into QCD [7,13] from such studies. A somewhat more mundane but still quite important task is to reduce uncertainties, due to our lack of knowledge of the parton content of the photon, in predictions of hadronic backgrounds at future high-energy e^+e^- [14,15] and ep colliders.

All existing theoretical estimates [1] of resolved photon cross sections make use of the Weizsäcker-Williams or effective photon approximation [16] to translate $\gamma\gamma$ and γp cross sections into e^+e^- and ep cross sections. The same formalism has been used when data [2–6] have been compared to theoretical expectations. Assuming that experimental (anti)tagging requirements as well as nonlogarithmic terms in the photon flux function are properly taken into account this approximation has been shown [17–19] to reproduce quite accurately exact calculations of processes where the photon participates directly, i.e., is not resolved into its hadronic substructure. However, no such check exists for resolved photon processes. Such a check would necessitate a complete understanding of the dependence of the parton content of the photon on the photon's virtuality P^2. While this dependence is computable [20,21] from pertubative QCD for large $P^2 \gg \Lambda^2$, and can be assumed to be negligible for $P^2 \ll \Lambda^2$, no satisfying treatment for the transiton region $P^2 \sim \Lambda^2$ exists. On the other hand, since contributions from far off-shell photons are suppressed by the photon propagator $1/P^2$, the contribution from $P^2 \sim \Lambda^2$ (or less) is usually numerically more important than the theoretically clean high-P^2 region.

In Ref. [14] we gave a first crude estimate of the suppression due to the virtuality of the exchanged photon. Here we attempt a more careful treatment, making use of recent results by Borzumati and Schuler [21], who pointed out that quark and gluon densities should be treated separately, the suppression being more severe in the latter case. Since the region of intermediate P^2 cannot (yet) be treated rigorously we use several simple *Ansätze* that contain one free parameter and reproduce the correct high-P^2 limit. We compare these with parameter-free predictions based on simple quark-parton model (QPM) calculations, and find reasonable agreement.

The remainder of this paper is organized as follows. In Sec. II we describe the general framework, taking care to treat experimental (anti)tagging of outgoing electrons properly. In Secs. III and IV this formalism is applied to quark and gluon densities, respectively. In all cases we were able to express the experimentally relevant quantity, the parton density (flux) function "in" the electron, in terms of a single integral to be computed numerically; the resulting expressions for cross sections are then as readily treatable as existing ones that ignore the virtuality of the exchanged photons. In Sec. V some numerical results are presented. Not surprisingly, antitagging, which imposes an upper limit on P^2, reduces the suppression, and it vanishes altogether if a forward tagger is used (as is done by the HERA experiments). A recently installed small angle electron detector should be able to study virtual photon effects in some detail, when combined with the existing forward tagger. Finally, Sec. VI contains a brief summary and some conclusions.

II. GENERAL FORMALISM

Since quite detailed discussions of the Weizsäcker-Williams approximation already exist in the literature

[22,23,17,24] we can be brief in this section. Consider a reaction that proceeds via the exchange of a photon in the t or u channel, $e + X \to e + X'$. In the effective photon approximation the corresopnding cross section is then written as

$$d\sigma(eX \to eX') \simeq f_{\gamma/e}(x_\gamma) dx_\gamma d\sigma(\gamma X \to X'), \quad (1)$$

where $x_\gamma \equiv E_\gamma/E_e$ is the scaled photon energy. This approximation is valid if (i) the contribution from the exchange of longitudinal photons is negligible and (ii) for the bulk of the contribution to the exact cross section the photon virtuality P^2 is small compared to the scale Q^2 characterizing the process $\gamma + X \to X'$.

These conditions are necessary since Eq. (1) expresses the cross section for eX scattering in terms of a cross section for γX scattering where the photon is *on-shell*, i.e., purely transverse.

If these conditions are fulfilled the photon flux can be written as [24,19]

$$f_{\gamma/e}(x_\gamma) = \int_{P^2_{\min}}^{P^2_{\max}} \frac{dP^2}{P^2} \tilde{f}(x_\gamma) - \frac{\alpha}{\pi} m_e^2 x_\gamma \left(\frac{1}{P^2_{\min}} - \frac{1}{P^2_{\max}} \right) , \quad (2)$$

where m_e is the electron mass and

$$\tilde{f}(x_\gamma) = \frac{\alpha}{2\pi x_\gamma} [1 + (1 - x_\gamma)^2] . \quad (3)$$

The kinematical limits on the virtuality are

$$P^2_{\min,\mathrm{kin}} = m_e^2 \frac{x_\gamma^2}{1 - x_\gamma}; \quad (4a)$$

$$P^2_{\max,\mathrm{kin}} = 0.5 s (1 - x_\gamma)(1 - \cos\theta_{\max}), \quad (4b)$$

where s is the squared center-of-mass energy of the eX system. In Eq. (4b) we have allowed for antitagging by introducing a maximal scattering angle $\theta_{\max}$ of the outgoing electron (in the eX cms frame). Similarly, small-angle tagging might introduce a lower bound on the virtuality, $P^2_{\min,\mathrm{tag}}$ that supersedes (4a). Moreover, condition (ii) implies that the *Ansatz* (1) breaks down if $P^2 > Q^2$; this has been confirmed in studies [18,19] where Eqs. (1)–(3) were compared to exact calculations of $d\sigma(eX \to eX')$. Altogether one thus has

$$f_{\gamma/e}(x_\gamma) = \tilde{f}(x_\gamma) \ln \frac{P^2_{\max}}{P^2_{\min}} + f_{\mathrm{rest}}(x_\gamma) , \quad (5)$$

with

$$P^2_{\min} = \max(P^2_{\min,\mathrm{kin}}, P^2_{\min,\mathrm{tag}}) , \quad (6a)$$

$$P^2_{\max} = \min(P^2_{\max,\mathrm{kin}}, \kappa Q^2) , \quad (6b)$$

$$f_{\mathrm{rest}}(x_\gamma) = -\frac{\alpha}{\pi} \frac{1 - x_\gamma}{x_\gamma} \text{ if } P^2_{\min,\mathrm{tag}} = 0 = 0 \text{ if } P^2_{\min,\mathrm{tag}} \gg m_e^2 , \quad (6c)$$

where κ is a number of order 1. For processes where the photon participates directly in the hard scattering reaction, rather than via its partonic constituents, the proper value of κ can be determined by comparing Eq. (1) with the result of an exact calculation at a few phase space points. However, in case of the resolved processes of interest for this paper the exact value of κ is not very important, since contributions from the region $P^2 \simeq P^2_{\max}$ are strongly suppressed anyway; in particular one should not expect to be able to estimate the precision of the estimate by varying κ around unity. In the following we therefore set $\kappa = 1$ for simplicity. Finally, in writing Eq. (6c) we have assumed $P^2_{\max} \gg m_e^2$, which is true for all applications at present high energy experiments.

The result (5) has been derived from Eq. (2) under the assumption that the only relevant P^2 dependence is contained in the explicit factor $1/P^2$. The standard procedure for treating resolved photon interactions [1] is to use Eq. (5) to define a parton density inside the electron:

$$f_{i|e}(y, Q^2) = \int_y^1 \frac{dx}{x} f_{\gamma/e}\left(\frac{y}{x}\right) f_{i|\gamma}(x, Q^2) , \quad (7)$$

where $f_{i|\gamma}(x, Q^2)$ is the probability to find parton i with momentum fraction x in a *real* photon when probed at scale Q^2. The cross section is then

$$d\sigma_{\mathrm{res}}(eX \to eX') = \sum_{i=q,G} f_{i|e}(x, Q^2) dx d\sigma(iX \to X') . \quad (8)$$

The point we wish to make in this paper is that in case of resolved photon interactions there is additional P^2 dependence beyond the $1/P^2$ factor contained in Eq. (2). Of course, the exact cross section (1) will always contain additional P^2 dependence; however, in many cases this dependence appears as terms $\propto (P^2/Q^2)^{n>0}$, which can be neglected if condition (ii) is satisfied. The crucial difference in case of resolved photon interactions is that they introduce an additional (hadronic) scale, very roughly characterized by the QCD scale parameter Λ. This opens the possibility that terms $\propto (P^2/\Lambda^2)^n$ appear, which are *not* always small even if (ii) is fulfilled. As we will see below, there is good reason to believe that the leading P^2 dependence is logarithmic; in other words, when writing Eq. (7) one ignores terms $\propto \ln(P^2/\Lambda^2)$, which may not be negligible compared to the leading terms $\propto \ln(Q^2/\Lambda^2)$.

Fortunately we need not give up the effective photon approximation altogether, since terms of the form $\ln(P^2/\Lambda^2)$ can *only* originate from the P^2 dependence of the parton densities $f_{i|\gamma}$. We can therefore generalize Eqs. (5) and (7) in a straightforward manner:

$$f_{i|e}(y, Q^2) = \int_y^1 \frac{dx}{x} \left[\tilde{f}\left(\frac{y}{x}\right) \int_{P^2_{\min}}^{P^2_{\max}} \frac{dP^2}{P^2} f_{i|\gamma}(x, Q^2, P^2) + f_{\mathrm{rest}}\left(\frac{y}{x}\right) f_{i|\gamma}(x, Q^2, 0) \right] , \quad (9)$$

where we have made use of the fact that $f_{\rm rest}$ is nonnegligible only if $P^2_{\rm min} \ll \Lambda^2$ so that real photon structure functions can be used in the second term in Eq. (9). This second term is thus the same as in Eq. (5) and (7); for simplicity we will omit it from our subsequent expressions, although it will be included in our numerical results. It reduces the parton content in the photon by typically 5 to 10% for Q^2 values of present interest and small or moderate values of y.

The first term in Eq. (9) involves a double integral, as opposed to the single integral in the standard form (7). In order to make further progress we must make some assumption regarding the P^2 dependence of the $f_{i|\gamma}$. As emphasized in Ref. [21] this dependence is quite different for quarks and gluons; in the next two sections we therefore discuss these two cases separately.

III. THE QUARK DENSITY IN THE ELECTRON

As mentioned above, the functions $f_{i|\gamma}(x, Q^2, P^2)$ can be computed unambiguously from perturbative QCD in the kinematic region $Q^2 \gg P^2 \gg \Lambda^2$. Since a detailed literature on this topic already exists [20,21] we do not repeat this calculation here. The result is that the parton densities are suppressed at high P^2 compared to the case of real photons; this is not surprising since a nonvanishing virtuality of the photon implies a lower limit for the virtuality of the partons in that photon. Unfortunately these rigorous, perturbative results are not applicable in the region $P^2 \simeq \Lambda^2$. As discussed in the Introduction we expect the contribution from this intermediate region to the inner integral in Eq. (9) to be at least as important numerically as the contribution from the high-P^2 region, due to the factor of $1/P^2$. Rather than attempting to accurately reproduce the (x-dependent) suppression at large P^2 as predicted [20,21] by QCD, we therefore use simple *Ansätze* which interpolate between the regions of low and high P^2.

We were guided by the observation of Borzumati and Schuler [21] that the parton densities inside a virtual photon approach the value predicted by the simple QPM in the limit $P^2 \to Q^2$, while the P^2 dependence disappears for $P^2 \ll \Lambda^2$. The simplest *Ansatz* that incorporates this behavior is

$$f^{(1)}_{q|\gamma}(x, Q^2, P^2) = q^\gamma(x, Q^2) \ , \quad P^2 \le P_c^2$$
$$= c_q(x, Q^2) \ln \frac{Q^2}{P^2} \ , \quad P^2 \ge P_c^2 \ , \qquad (10)$$

where $q^\gamma(x, Q^2)$ are the standard quark density functions in real photons [7]. Continuity of the *Ansatz* (10) at $P^2 = P_c^2$ implies

$$c_q(x, Q^2) = \frac{q^\gamma(x, Q^2)}{\ln(Q^2/P_c^2)}. \qquad (11)$$

In Eq. (10) we are trying to describe the intricacies of nonperturbative QCD in terms of a single parameter P_c. Clearly this cannot reproduce the exact P^2 dependence very accurately, nor will it reproduce the proper x dependence at a fixed value of P^2. However, here we are only interested in the integral over P^2 contained in Eq. (9). Given that our *Ansatz* (10), as well as other *Ansätze* to be described below, show the correct limiting behavior predicted by QCD it seems reasonable to believe that these P^2 integrals will indeed be described more or less correctly, if P_c is chosen to be a typical hadronic scale, i.e., between a few hundred MeV and a GeV.

Unlike the authors of Ref. [25] we do not distinguish between "soft" and "hard" components of the photon structure functions, where the soft component [to be estimated from the vector dominance model (VDM)] would be suppressed by a power of P^2 (rather than logarithmically) at high P^2. In this picture one assumes that the hard component is zero at some rather low input scale Q_0^2, i.e., that at this scale the photon is indeed identical to a vector meson as far as its hadronic properties are concerned. It is not clear to us whether this amalgam of the VDM and QCD is meaningful. In any case, such a soft component could easily be incorporated in our framework. As shown in Ref. [25], for this soft part itself virtual photon effects can to good approximation be included by simply cutting off the P^2 integral in Eq. (9) at some scale $\simeq m_\rho^2 \simeq 0.5$ GeV^2. Our subsequent results would then only be valid for the hard part of the photon structure functions, which can be obtained by subtracting pionlike parton densities from standard parametrizations [8–12] of q^γ.

Inserting Eqs. (10) and (11) into (9) gives (recall that we omit the term $\propto f_{\rm rest}$ here)

$$f^{(1)}_{q|e}(y) = \int_y^1 \frac{dx}{x} \tilde{f}\left(\frac{y}{x}\right) q^\gamma(x, Q^2) \left[\ln \frac{\min(P_c^2, P^2_{\rm max})}{P^2_{\rm min}} + \frac{1}{2}\theta(P^2_{\rm max} - P_c^2)\left(\ln \frac{Q^2}{P_c^2} - \frac{\ln^2(Q^2/P^2_{\rm max})}{\ln(Q^2/P_c^2)} \right) \right] , \qquad (12)$$

where $\tilde{f}$ has been defined in Eq. (3). This expression is completely general; in particular, it allows to take (anti)tagging into account via its effects on $P^2_{\rm min}$ and $P^2_{\rm max}$, see Eqs. 6(a) and 6(b). In the important special case where there is no antitagging, i.e., where $P^2_{\rm max} = Q^2$, Eq. (12) simplifies to

$$f^{(1),\text{no-tag}}_{q|e}(y) = \int_y^1 \frac{dx}{x} \tilde{f}\left(\frac{y}{x}\right) q^\gamma(x, Q^2) \ln \frac{Q^2}{P^2_{\rm min}} \left[1 - \frac{1}{2} \frac{\ln(Q^2/P_c^2)}{\ln(Q^2/P^2_{\rm min})} \right] . \qquad (13)$$

Notice that the integrands in Eqs. (12) and (13) factorize into a parton density (a function of x) and a photon flux factor (a function of x/y) only if P_c is a constant, independent of x [recall that $P^2_{\rm min}$ depends on the scaled photon energy y/x, see Eq. (4a)]. However, even in the general case where this factorization is lost $f_{q|e}$ is still given by a single integral, just like in Eq. (7) where virtual photon effects have been ignored.

Equations (10)–(12) can be used by simply assuming a constant value for P_c; since it characterizes a typical hadronic scale, it should roughly lie in the range

$$\Lambda^2 \leq P_c^2 \leq m_p^2 \,. \tag{14}$$

Alternatively, one might try to estimate P_c from the QPM; after all, the *Ansatz* (10) was motivated by the QPM. One has (for quark mass $m_q^2 \ll P^2$)

$$\begin{aligned} f_{q|\gamma}^{\mathrm{QPM}}(x,Q^2,P^2) &= 3\frac{\alpha}{2\pi}e_q^2[x^2+(1-x)^2]\ln\frac{Q^2}{P^2} \\ &\equiv c_q^{\mathrm{QPM}}\ln\frac{Q^2}{P^2}\,, \end{aligned} \tag{15}$$

which has the form of Eq. (10). The QPM therefore makes a prediction for c_q, so that Eq. (11) can be solved for $\ln(Q^2/P_c^2)$; the solution will in general depend on x and Q^2.

The main advantage of the *Ansatz* (10) is its simplicity. However, when plotted vs $\ln P^2$ it shows an ugly kink, i.e., the derivative $\partial f_{q|\gamma}/\partial \ln P^2$ is discontinuous at $P^2 = P_c^2$. This drawback can be overcome by writing

$$f_{q|\gamma}^{(2)}(x,Q^2,P^2) = q^\gamma(x,Q^2)\frac{\ln\frac{Q^2+P_c^2}{P^2+P_c^2}}{\ln(1+Q^2/P_c^2)}\,. \tag{16}$$

This modified *Ansatz* has the same behavior as Eq. (10) in the limits $P^2 \to 0$ and $P^2 \to Q^2$, but smoothly interpolates between these two limits at $P^2 \simeq P_c^2$. Strictly speaking Eq. (16) does not allow us to express the P^2 integral in Eq. (9) in terms of elementary functions. However, one can derive an excellent analytical approximation to the exact result by splitting the P^2 integration into the domains $P^2 \leq P_c^2$ and $P^2 > P_c^2$, using two different expansions for $\ln(P^2+P_c^2)$ in these integration regions. The result is (for $P_{\max}^2 > P_c^2$)

$$f_{q|e}^{(2)}(y) = \int_y^1 \frac{dx}{x}\tilde{f}\left(\frac{y}{x}\right)q^\gamma(x,Q^2)\left[\ln\frac{P_c^2}{P_{\min}^2}+\frac{1}{2}\ln\left(1+\frac{Q^2}{P_c^2}\right)+\frac{P_c^2/P_{\max}^2+P_{\min}^2/P_c^2-\pi^2/6-0.5\ln^2\frac{Q^2+P_c^2}{P_{\max}^2}}{\ln(1+Q^2/P_c^2)}\right]. \tag{17}$$

This result is exact up to terms $O\left(\frac{P_c^4}{P_{\max}^4},\frac{P_{\min}^4}{P_c^4}\right)$; it reproduces the numerical result to better than 2% for all cases we tried.

Before presenting numberical predictions we now turn to a discussion of gluon densities.

IV. THE GLUON DENSITY IN THE ELECTRON

Unfortunately the simple *Ansatz* (10) will not do for the case of gluons. The reason is that, as emphasized in Ref. [21], $f_{G|\gamma}(x,Q^2,P^2)$ vanishes faster than $\ln(Q^2/P^2)$ as $P^2 \to Q^2$. This can be understood perturbatively from the observation that a gluon has to be radiated from a quark which is itself off-shell if $P^2 \neq 0$. One should thus be able to find a reasonable *Ansatz* for $f_{G|\gamma}(x,Q^2,P^2)$ by considering a diagram where a photon splits into a $q\bar{q}$ pair and one of the quarks radiates a gluon. Let q_1^2 and q_2^2 be the virtualities of the emitting (anti)quark and gluon, respectively; in the spirit of the backward showering algorithm [26] this gives for the gluon density

$$f_{G|\gamma}(x,Q^2,P^2) \propto \int_{P^2}^{Q^2}\frac{dq_1^2}{q_1^2}\int_{q_1^2}^{Q^2}\frac{dq_2^2}{q_2^2}\alpha_s\,. \tag{18}$$

The result will obviously depend on the choice of momentum scale in α_s, which is ambiguous within the leading logarithmic approach followed here. However, we know that the gluon density must vanish at least $\propto \ln^2(Q^2/P^2)$ as $P^2 \to Q^2$; on the other hand, for $Q^2 \gg P^2$ we want to reproduce the well-known result [7] that $f_{g|\gamma}$ grows like $\ln Q^2$. Choosing α_s in Eq. (18) to be independent of q_1^2 and q_2^2 gives $f_{G|\gamma} \propto \alpha_s \ln^2(Q^2/P^2)$, which has the correct high-Q^2 behavior only if we take the scale in α_s to be Q^2. This motivates the *Ansatz*

$$\begin{aligned} f_{G|\gamma}^{(1a)}(x,Q^2,P^2) &= G^\gamma(x,Q^2)\,, \quad P^2 \leq P_c^2 \\ &= c_G(x,Q^2)\frac{\ln^2(Q^2/P^2)}{\ln(Q^2/\Lambda)}\,, \quad P^2 \geq P_c^2\,, \end{aligned} \tag{19}$$

where $G^\gamma(x,Q^2)$ is the gluon distribution function for on-shell photons. Continuity at $P^2 = P_c^2$ requires that

$$c_G(x,Q^2) = G^\gamma(x,Q^2)\frac{\ln(Q^2/\Lambda^2)}{\ln^2(Q^2/P_c^2)}\,, \tag{20}$$

which can easily be solved for P_c^2 if c_G is known (see below).

One obtains a slightly more complicated *Ansatz* if α_s in Eq. (18) is taken to depend on q_1^2 or q_2^2. Choosing q_1^2 as scale of α_s leads to a result that grows faster than $\ln Q^2$ for large Q^2, which is not acceptable. Taking q_2^2 as scale does lead to a reasonable *Ansatz*, however,

$$\begin{aligned} f_{G|\gamma}^{(1b)}(x,Q^2,P^2) &= G^\gamma(x,Q^2)\,, \quad P^2 \leq P_c^2 \\ &= c_G(x,Q^2)\left[\ln\frac{Q^2}{P^2}-\ln\frac{P^2}{\Lambda^2}\ln\left(\frac{\ln(Q^2/P^2)}{\ln(Q^2/\Lambda^2)}\right)\right]\,, \quad P^2 \geq P_c^2\,. \end{aligned} \tag{21}$$

In this case the continuity condition at $P^2 = P_c^2$ can still easily be solved for $c_G(x,Q^2)$, but an explicit analytical expression for P_c^2 for given c_G is no longer possible.

Both the *Ansatz* (19) and (21) allow to compute the P^2 integral in Eq. (9) analytically. In the former case one has

$$f_{G|e}^{(1a)}(y) = \int_y^1 \frac{dx}{x} \tilde{f}\left(\frac{y}{x}\right) G^\gamma(x,Q^2) \left[\ln\left(\frac{\min(P_c^2, P_{\max}^2)}{P_{\min}^2} \right) + \frac{1}{3}\theta(P_{\max}^2 - P_c^2) \left(\ln\frac{Q^2}{P_c^2} - \frac{\ln^3(Q^2/P_{\max}^2)}{\ln^2(Q^2/P_c^2)} \right) \right] . \tag{22}$$

In a no-tag situation, $P_{\max}^2 = Q^2$, this simplifies to

$$f_{G|e}^{(1a),\text{no-tag}}(y) = \int_y^1 \frac{dx}{x} \tilde{f}\left(\frac{y}{x}\right) G^\gamma(x,Q^2) \ln\frac{Q^2}{P_{\min}^2} \left[1 - \frac{2}{3} \frac{\ln(Q^2/P_c^2)}{\ln(Q^2/P_{\min}^2)} \right] . \tag{23}$$

Note the similarity to the corresponding result (13) for $f_{q|e}$. However, the stronger suppression of the gluon density at large P^2 leads to a larger coefficient of the subtraction term in the square bracket (2/3 rather than 1/2).

The somewhat more complicated *Ansatz* (21) gives (for $P_{\max}^2 > P_c^2$)

$$f_{G|e}^{(1b)}(y) = \int_y^1 \frac{dx}{x} \tilde{f}\left(\frac{y}{x}\right) \left\{ G^\gamma(x,Q^2) \ln\frac{P_c^2}{P_{\min}^2} + \frac{1}{2} c_G(x,Q^2) \left[\ln^2\frac{Q^2}{P_c^2} - \ln^2\frac{Q^2}{P_{\max}^2} + \ln^2\frac{P_c^2}{\Lambda^2} \left(\ln\left(\frac{\ln(Q^2/\Lambda^2)}{\ln(P_c^2/\Lambda^2)} \right) + \frac{1}{2} \right) \right.\right.$$
$$\left.\left. - \ln^2\frac{P_{\max}^2}{\Lambda^2} \left(\ln\left(\frac{\ln(Q^2/\Lambda^2)}{\ln(P_{\max}^2/\Lambda^2)} \right) + \frac{1}{2} \right) \right] \right\} . \tag{24}$$

This expression also simplifies somewhat in the no-tag case $P_{\max}^2 = Q^2$, but one does not recover a result as simple as Eq. (13) or (23). Of course, in Eq. (24) $c_G(x,Q^2)$ is related to P_c^2 and $G^\gamma(x,Q^2)$ via the continuity condition at $P^2 = P_c^2$.

As in case of the quark density, c_G can be obtained from a simple parton-level calculation. Specifically, in the picture of a photon to quark to gluon splitting used in deriving Eq. (18) one finds the following x dependence:

$$c_G^{\text{QPM}}(x) \propto \int_x^1 \frac{dy}{y} c_q^{\text{QPM}}(y) P_{Gq}\left(\frac{x}{y}\right) = N \left[\frac{4}{3}\left(\frac{1}{x} - x^2 \right) + 1 - x + 2(1+x)\ln x \right] , \tag{25}$$

where P_{Gq} is the quark→gluon splitting function [27]. The normalization N of c_G^{QPM} can be fixed from the result (15) for c_q^{QPM}, taking into account that the dependence on P^2 and Q^2 has already been factored out in the *Ansatz* (19):

$$N = \frac{\alpha}{\pi} \frac{6}{33 - 2N_f} \sum_{q,\bar{q}} e_q^2 , \tag{26}$$

where N_f is the number of active flavors. Together with continuity relation (20), Eqs. (25) and (26) can again be used to determine P_c for given x and Q^2; of course, the result will depend on $G^\gamma(x,Q^2)$, which is still not very well determined experimentally [1].

Both Eqs. (19) and (21) suffer from the same problem as the simple *Ansatz* (10) for $f_{q|\gamma}$: The derivative with respect to $\ln P^2$ is discontinuous at $P^2 = P_c^2$. This can be solved in complete analogy to Eq. (16) by modifying the *Ansatz* for $f_{G|\gamma}$ to

$$f_{G|\gamma}^{(2)}(x,Q^2,P^2) = G^\gamma(x,Q^2) \frac{\ln^2 \frac{Q^2+P^2}{P^2+P_c^2}}{\ln^2\left(1 + \frac{Q^2}{P_c^2}\right)} . \tag{27}$$

The same procedure that led to Eq. (17) again allows to find an excellent approximation for the P^2 integral in Eq. (9):

$$f_{G|e}^{(2)}(y) = \int_y^1 \tilde{f}\left(\frac{y}{x}\right) G^\gamma(x,Q^2) \left[\ln\frac{P_c^2}{P_{\min}^2} + \frac{1}{3}\ln\left(1 + \frac{Q^2}{P_c^2}\right) + \frac{2P_{\min}^2/P_c^2 - \pi^2/3}{\ln\left(1 + \frac{Q^2}{P_c^2}\right)} \right.$$
$$\left. + \frac{\frac{9}{4} - \frac{1}{3}\ln^3\frac{Q^2+P_c^2}{P_{\max}^2} + \frac{2P_c^2}{P_{\max}^2}\left(\ln\frac{Q^2+P_c^2}{P_{\max}^2} - 1 \right) + \frac{P_c^4}{2P_{\max}^4}\left(\frac{1}{2} - \ln\frac{Q^2+P_c^2}{P_{\max}^2} \right)}{\ln^2\left(1 + \frac{Q^2}{P_c^2}\right)} \right] , \tag{28}$$

where we have again assumed $P_{\max}^2 > P_c^2$, and terms of $\mathcal{O}\left(\frac{P_c^6}{P_{\max}^6}, \frac{P_{\min}^4}{P_c^4}\right)$ have been omitted. Numerically Eq. (28) reproduces the exact result in Eq. (9) to better than 2 %.

V. NUMERICAL EXAMPLES

We are now in a position to present numerical examples for $f_{i|e}$, using the results of Secs. III and IV. We start with two examples relevant for the e^+e^- collider TRISTAN, which now operates at $\sqrt{s} \simeq 57$ GeV. Here we are only interested in the reduction of the expected parton flux due to the virtuality of the exchanged photons as well as due to experimental (anti)tagging conditions. We therefore normalize our results to the most naive "unsuppressed" prediction for $f_{i|e}$, which has been obtained from Eqs. (7) and (5) with $P_{\max}^2 = s(1-x_\gamma)$ [Eq. (4b)

with $\theta_{max} = \pi$]. As already explained in Sec. II this *Ansatz* overestimates the correct parton flux even in the absence of antitagging and high-P^2 suppression, since the relevant scale Q^2 of the hard $\gamma\gamma$ scattering (to be identified, e.g., with the squared transverse momentum of high-p_T jets) is usually (much) smaller than $P^2_{max,kin}$.

In Figs. 1(a) (for u quarks) and 1(b) (for gluons) we have chosen $Q^2 = 10$ GeV^2, typical for current $\gamma\gamma$ data at TRISTAN [2,3]; no (anti)tagging has been required. The dotted curves show the reduction that results from imposing the dynamical bound $P^2 \leq Q^2$ on the virtuality of the exchanged photons. These curves are only slightly affected by the x dependence of the parton densities. For very large photon energy x_γ the kinematical constraint (4b) will give a bound below Q^2 even for $\theta_{max} = \pi$ (no tag); requiring $P^2 \leq Q^2$ does therefore not affect the flux of very energetic photons. If the parton density in the photon is very soft (concentrated at small x) the region of large x_γ will contribute more to the convolution integral defining $f_{i|e}$. Therefore the effect of requiring $P^2 \leq Q^2$ is slightly smaller for the (soft) gluon density than for the (hard) quark density.

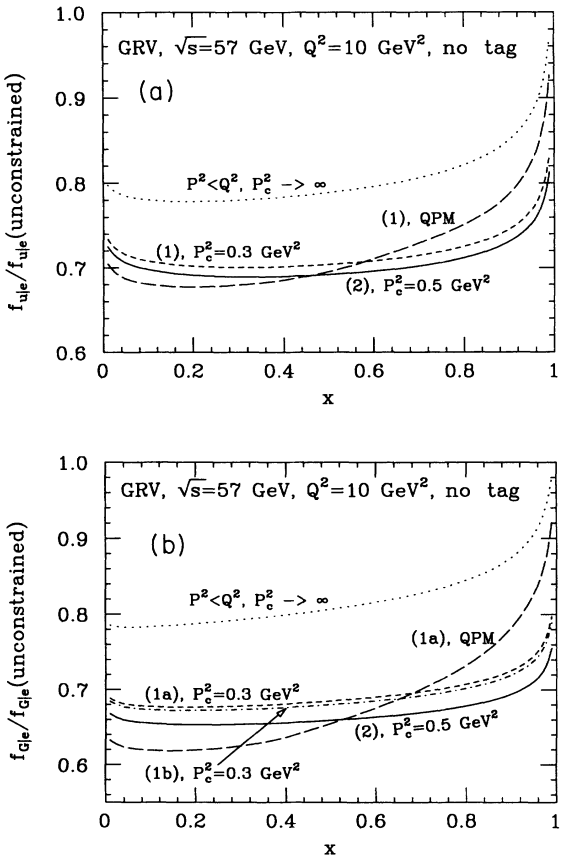

FIG. 1. The reduction of the parton density in the electron in a no-tag situation due to bound $P^2 \leq Q^2$ as well as due to the suppression of virtual photon structure functions. All curves are normalized to the parton densities obtained from Eqs. (4)–(7) with $\theta_{max} = \pi$, ignoring the condition (6b); (a) is for the u-quark density, while (b) is for the gluon density. The dotted curves show the effect of only requiring $P^2 \leq Q^2$, while the dashed and solid curves also include the suppression of $f_{i|\gamma}$ at $P^2 \neq 0$. In (a) the short dashed and long dashed curves represent the prediction (13) with fixed P_c^2 and with P_c^2 estimated from the QPM, respectively, while the solid line shows the result (17). In (b) the short dashed and long dashed curves depict the prediction (23) with fixed P_c^2 and with P_c^2 estimated from the QPM, respectively, while the dot-dashed and solid lines represent the predictions from Eqs. (24) and (28), respectively. The leading order parametrization of Ref. [10] has been used.

The solid and dashed curves in Fig. 1 show our estimates of the combined suppression due to the virtuality of the exchanged photons and the requirement $P^2 \leq Q^2$. The short dashed curve in Fig. 1(a) shows the prediction (13) of the simple *Ansatz* (10) with fixed $P_c^2 = 0.3$ GeV^2, while the long dashed curve is the prediction (13) if P_c^2 is estimated from the QPM using Eq. (15). The corresponding curves in Fig. 1(b) refer to the prediction (23) of the simple *Ansatz* (19) with fixed P_c^2, and with P_c^2 determined from the QPM results (25) and (26), respectively; the dot-dashed curve here show the prediction (24) of the somewhat more complicated *Ansatz* (21). In these figures the solid curve shows predictions [Eqs. (17) and (28)] of the smoothed-out *Ansätze* (16) and (27), respectively, where we have assumed $P_c^2 = 0.5$ GeV^2.

We see that all predictions for $f_{u|e}$ are quite similar. Notice, however, that we have used slightly different values for P_c^2 with the smooth *Ansätze* for $f_{i|\gamma}$ than for the simple ones whose derivatives are discontinuous. This is reasonable since the former predict some suppression for all $P^2 \neq 0$, while the latter assume $f_{i|\gamma}$ to be completely unsuppressed for $P^2 < P_c^2$. The fact that the results using the QPM estimate (15) come out quite close to the other predictions give us some confidence that our choices of P_c^2 are indeed reasonable. We should mention here that when using the QPM estimates we have always required $P_c^2 \geq \Lambda^2$, see Eq. (14), i.e., we have set $P_c^2 = \Lambda^2$ (= 0.04 GeV^2 for the GRV parametrization [10] used in Fig. 1) if the QPM predicts $P_c^2 < \Lambda^2$. In case of $f_{u|e}$ this happens only at small x, where (multiple) gluon radiation is expected to be important, so that the QPM prediction cannot be trusted. Note, however, that this result depends to some extent on the parametrization of the parton densities in the photon. For example, when used with the Drees-Grassie (DG) parametrization [8] the QPM predicts significantly less suppression of $f_{u|e}$ at large x. The reason is that this parametrization has a rather small u^γ at large x, which implies a large value of P_c^2, and hence little suppression, if c_u is fixed from the QPM, see Eq. (11). Moreover, our prediction for $f_{G|e}$ using the QPM-inspired *Ansatz* of Eqs. (25) and (26) does deviate somewhat from the other predictions. The reason is that, at least for the GRV parametrization [10], a good part of the gluon density at $Q^2 = 10$ GeV^2 still originates from the nonpertrubative input distribution, which cannot be expected to be described properly by a QPM *Ansatz*. Specifically, in the situation depicted in Fig. 1(b) this *Ansatz* always predicts a very small value of P_c^2; since we do not allow $P_c^2 < \Lambda^2$, in the region $x \leq 0.5$ the long-dashed curve in this figure is actually quite close to the corresonding result with fixed $P_c^2 = 0.04$ GeV^2.

Generally we conclude that in a no-tag situation with

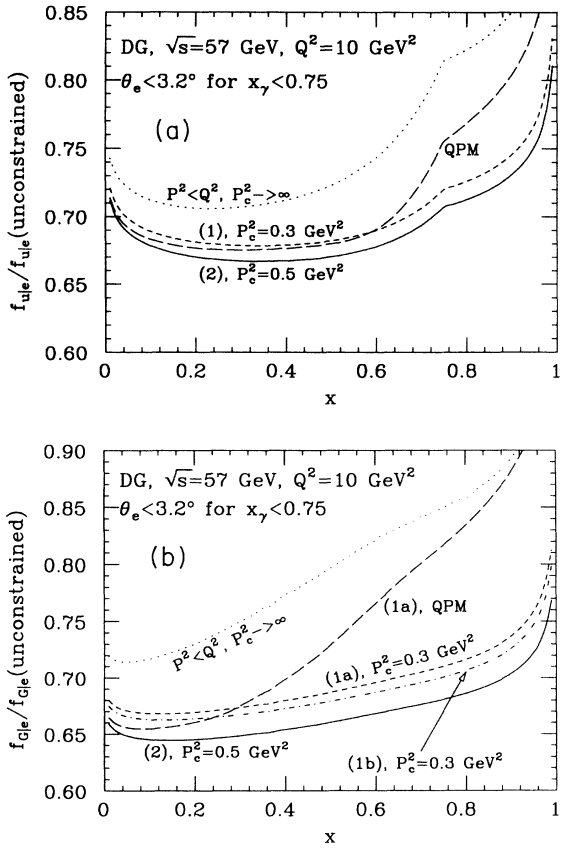

FIG. 2. The reduction of $f_{u|e}$ (a) and $f_{G|e}$ (b) for an antitag situation, i.e., Eq. (4b) has been used with $\theta_{\max} = 3.2°$ iff $x_\gamma \leq 0.75$. We have used the parametrization of Ref. [8]. Notations are as in Fig. 1.

$Q^2 = 10$ GeV^2 virtual photon effects suppress $f_{q|e}$ by 8 to 10% and $f_{G|e}$ by 12 to 15% even after the constraint $P^2 \leq Q^2$ has been included; one expects even larger suppression at larger Q^2, since then a larger fraction of the P^2 integral in Eq. (9) comes from the region $P^2 > P_c^2$ where the $f_{i|\gamma}$ are reduced significantly.[1] Apart from the region of large x, which contributes only little to any cross section becuase $f_{i|e} \to 0$ as $x \to 1$, the predicted suppression is almost independent of x if a fixed value of P_c^2 is assumed; this is not true if P_c^2 is estimated from the QPM, however.

In Figs. 2(a) and 2(b) we show corresponding results for an antitag situation; this might be more relevant for practical applications, since some (anti)tagging is usually applied in experimental analyses [2–4] of two-photon data, in order to separate events with low and high P^2. In these figures we have used the antitagging applied by the TOPAZ collaboration in their recent analysis of jet production in $\gamma\gamma$ collisions: $\theta_{\max} = 3.2°$ for scaled photon energy $x_\gamma \leq 0.75$, and $\theta_{\max} = \pi$ otherwise. For comparison with Fig. 1 we use the same "unconstrained" $f_{i|e}$ as before, where neither antitagging nor the bound $P^2 \leq Q^2$ has been taken into account. Both these constraints have been included in the dotted curves in Fig. 2, which (for $x_\gamma < 0.75$) therefore lie significantly below the corresponding curves in Fig. 1 where no antitagging was assumed. Notice, however, that antitagging has lowered our final result for the $f_{i|e}$ (solid and dashed curves), including virtual photon effects, by only 2–3% compared to Fig. 1. The reason is that the region $P^2 > P^2_{\max,\text{tag}}$ contributes relatively little to $f_{i|e}$ even in Fig. 1, due to the suppression of the $f_{i|\gamma}$ at these high P^2. Once antitagging has been taken into account, virtual photon effects suppress $f_{q|e}$ by only about 5%. In case of gluons, however, this additional reduction could be as large as 10% even in the region of small x where $f_{G|e}$ is sizable. Our antitagging condition is less effective for gluons since, as discussed above, $f_{G|e}$ gets a relatively larger contribution from the region of large x_γ than $f_{q|e}$ does. This demonstrates that the exact experimental implementation of antitagging is important. In the present case only electrons with energy $> E_{\text{beam}}/4$ are vetoed at large angles, which does not affect events where most of the energy of the incident electrons is carried away by the photon.

Notice also that the QPM prediction for $f_{G|e}$ [long dashed curve in Fig. 2(b)] now agrees quite well with the predictions for fixed P_c^2 at least in the region $x \leq 0.4$; this is becuase we have used the DG parametrization [8] here, whose gluon density is created purely radiatively. The QPM prediction differs strongly from the other results for $x > 0.5$. However, this region will not contribute much to any cross section, since this parametrization is characterized by a rather soft gluon distribution function. For practical purposes our different *Ansätze* for $f_{i|\gamma}$ therefore give quite similar results. In particular, $f_{G|e}^{(1b)}$ of Eq. (24) always comes out very close to $f_{G|e}^{(1a)}$ of Eqs. (22) and (23); the use of the somewhat more cumbersome *Ansatz* (21) for $f_{G|\gamma}$ therefore hardly seems worth the trouble, considering that it still suffers from a discontinuous derivative at $P^2 = P_c^2$.

Our final example concerns the small angle electron tagger that has recently been installed [28] in the ZEUS detector at the *ep* collider HERA. Unlike the forward taggers used by both HERA experiments [5,6], this detector is only sensitive to events with a finite, although small, photon virtuality: 0.1 GeV$^2 \leq P^2 \leq 1$ GeV^2. At HERA ($\sqrt{s} \simeq 296$ GeV at present) this implies $P^2_{\min,\text{tag}} = 0.1$ GeV$^2 > P^2_{\min,\text{kin}}$ and $P^2_{\max,\text{tag}} = 1.0$ GeV$^2 < P^2_{\max,\text{kin}}$ for almost all photon energies. The predicted suppression of the $f_{i|e}$ due to virtual photon effects is therefore independent of x if one of our *Ansätze* is used with fixed P_c^2.

The suppression does depend on the scale Q^2 characterizing γp scattering, however. This is demonstrated in Fig. 3, where we show the suppression of $f_{u|e}$ (solid) and $f_{G|e}$ (dashed) for $P_c^2 = 0.15$ and 0.5 GeV^2, as predicted from the simple *Ansätze* (10) and (19). In contrast to the situation depicted in Fig. 1 the suppres-

[1] In order to avoid confusion we should mention that the absolute values of the $f_{i|e}$ still increase with increasing Q^2 even after the suppression of virtual photon structure functions has been taken into account. However, the increase is slower than one would expect in the absence of this suppression; therefore in a no-tag situation the suppression becomes relatively more important at larger Q^2.

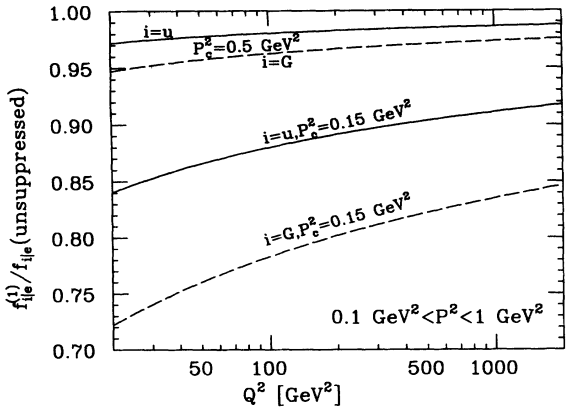

FIG. 3. The reduction of the parton flux in the electron due to the suppression of $f_{i|\gamma}(P^2 \neq 0)$ if the photon virtuality is restricted to lie in the range 0.1 GeV^2 $\leq P^2 \leq$ 1.0 GeV^2, predicted from Eqs. (12) (for $f_{u|e}$, solid curves) and (22) (for $f_{G|e}$, dashed) with fixed P_c^2. Since the limits on P^2 are independent of x the reduction of the parton fluxes also does not depend on x, nor on the parametrization of real photon structure functions chosen. It does, however, depend on the scale Q^2 at which the photon is being probed, as shown in the figure. This suppression should be measurable at the ZEUS detector at HERA, as discussed in the text.

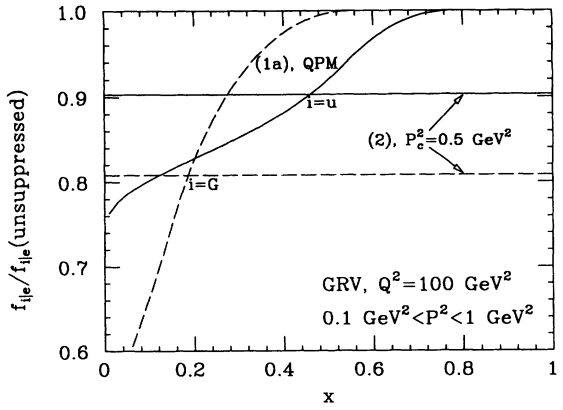

FIG. 4. The x dependence of the suppression of the parton fluxes for the same kinematical constraints as in Fig. 3, for Q^2 = 100 GeV^2 and the Glück-Reya-Vogt (GRV) parametrization [10]. The horizontal lines show the suppression as predicted from Eqs. (17) (solid, for u quarks) and (27) (dashed, for gluons), respectively, while the other two curves show predictions of the QPM-inspired *Ansätze* (15) and (25), respectively.

sion now decreases with increasing Q^2. The reason is that here, unlike in Fig. 1, the upper limit of the P^2 integration in Eq. (9) is simply fixed by the experimental tagging condition, which is independent of Q^2. The behavior depicted in Fig. 3 then follows from the fact that $f_{i|\gamma}(P^2 > P_c^2)$ is relatively less suppressed at larger Q^2. Experimentally Q^2 can, e.g., be identified with the squared transverse momentum of high-p_T jets produced in the event. The ratio shown in Fig. 3 can therefore be measured experimentally by comparing the rate for jet events where the electron is detected in the small angle tagger to that where the electron hits the forward spectrometer presently used for tagging photoproduction events (and for measuring the luminosity); this forward spectrometer only accepts events with $P^2 < 0.1$ GeV^2, where the virtuality of the photon should indeed be negligible.[2] This measurement should be very clean since by comparing events with equal characteristics of the hadronic system (p_T and rapidity of the jets) and with equal energy of the tagged electron most hadronic uncertainties, e.g., related to unknown structure functions, will cancel out.

As usual we find larger suppression for the gluon density than for quark densities. Notice that on average gluon-induced jet events look quite different from quark-induced and direct events [29]: The high-p_T jets tend to emerge at larger rapidities, closer to the proton beam direction; and they tend to have more energetic photon remnant jets. Since going to finite P^2 suppresses gluon-induced processes more than quark-induced processes while direct processes are not suppressed at all (apart from the trivial reduction of $f_{\gamma/e}$) we expect the high-p_T jets in events tagged by the small angle tagger to be on average more central, compared to events tagged by the forward spectrometer; similarly, the former class of events should on average have somewhat less hadronic activity from the photon remnants in the electron beam direction. These qualitative effects can unambiguously be predicted from QCD, which requires $f_{G|e}$ to be more strongly suppressed than $f_{q|e}$ [21]; however, Fig. 3 shows that the size of these effects depend on the nonperturbative parameter P_c^2, which at present cannot be predicted from first principles. We should mention here that we regard the values of P_c^2 chosen in Fig. 3 to approximate the lower and upper bounds of the range of reasonable values; our "best guess," corresponding to the value chosen in Figs. 1 and 2, would fall roughly halfway in between these two.

Finally, in Fig. 4 we show the x-dependent suppression of the $f_{i|e}$ as predicted by the QPM-inspired *Ansätze* (15) and (25) when used in combination with the GRV parametrization, again for events tagged by the small angle tagger with Q^2 = 100 GeV^2; the (x independent) suppression predicted by the *Ansätze* (16) and (27) are shown for comparison. We see that the QPM *Ansätze* predict a rather strong x dependence of the suppression factor, especially for $f_{G|e}$. However, in this case we have $Q^2 \gg P_{\max}^2$, leaving plenty of phase space for the emission of additional gluons, which shift parton densities from large to small x values. It is therefore not surprising that the QPM *Ansätze* overestimate the parton densities at large x (where they predict $P_c^2 > 1$ GeV^2 and hence no suppression in the present case) and underestimate

[2]The effective photon flux for events tagged by the forward spectrometer is considerably larger than for events tagged by the small angle tagger; in the former case, $\ln(P_{\max}^2/P_{\min}^2) \simeq$ 13, compared to 2.3 for the latter. One can easily correct for this known difference in photon fluxes to determine the suppression due to the virtuality of the photon, shown in Fig. 3.

them at small x (where they predict $P_c^2 < \Lambda^2$, which we have again interpreted to mean $P_c^2 = \Lambda^2 = 0.04$ GeV^2).

VI. SUMMARY AND CONCLUSIONS

In this paper we have studied the reduction of the effective parton flux in the electron due to experimental (anti)tagging, as well as due to the suppression of virtual photon structure functions compared to the more familiar structure functions of real (on-shell) photons. Our mains results are given in Eqs. (12) and (17) for quark densities and Eqs. (22), (24), and (28) for gluon densities. These effects treat the dependence of photon structure functions on the virtuality P^2 of the photon only in an approximate manner; however, we argued in Sec. III that they ought to reproduce the relevant integrals over P^2 quite accurately, since they are based on parametrizations of the parton content of virtual photons that have the correct low and high P^2 limits. The virtue of this simplified approach is that it still allows to express the effective parton densities in the electron in terms of a single convolution integral, similar to the standard expression (7) where the reduction of virtual photon structure functions is ignored. These parton densities in the electron directly enter predictions for cross sections of resolved photon processes, as shown in Eq. (8).

In our numerical examples of Sec. V we found that the size of the suppression depends both on the experimental (anti)tagging requirements and on the scale Q^2 at which the photon is probed. In a no-tag situation Q^2 provides the upper limit on P^2, since for $P^2 > Q^2$ it no longer makes sense to describe the process in terms of partons "in" the (virtual) photon. In this situation increasing Q^2 gives more relative weight to the region of large (compared to Λ^2) photon virtualities, and hence leads to larger suppression factors. Conversely, if experimental (anti)tagging determines the upper bound on P^2, increasing Q^2 will reduce the suppression factor since the relative (to Q^2) virtuality of photons in accepted events is reduced.

Present $\gamma\gamma$ experiments are now analyzing data with Q^2 typically around 10 GeV^2. We estimate that in a no-tag situation virtual photon effects then suppress the effective quark and gluon content by about 10 and 15%, respectively; note that the reduction of cross sections of twice-resolved $\gamma\gamma$ processes is twice as large, since they contain two factors of $f_{i|e}$. Under experimentally more relevant antitagging conditions we estimate the suppression of quark densities to be a modest 2–3%, which is hardly significant compared to other experimental and theoretical uncertainties; however, gluon densities could still be reduced by 10%, an effect similar in size to the recent computed next-to-leading-order (NLO) corrections to jet production in real $\gamma\gamma$ scattering [25].

We finally pointed out that the small angle electron tagger recently installed in the ZEUS experiment at HERA should allow us to study the onset of the suppression of virtual photon structure functions in some detail. Hadronic uncertainties can largely be removed by comparing the rate of events tagged by this device to that tagged by the existing forward spectrometer. Our "best guess" for the suppression at $Q^2 = 100$ GeV^2 is around 8 and 15% for quark- and gluon-initiated processes, respectively. The stronger suppression of the rate of events with a gluon from the photon in the initial state should lead to changes in the average rapidity of the hard jets as well as the average energy of the photon remnant. We remind the reader here that we ignored the possible existence of a "soft" contribution to the photon structure function. Such a contribution would be much more strongly suppressed at high P^2, and should therefore be easily detectable by this small angle tagger.

In summary, effects due to the suppression of virtual photon structure functions are of roughly comparable size as NLO QCD corrections in a no-tag experiment; they are somewhat smaller, but can still be non-negligible, when antitagging is imposed. They should therefore be taken into account when one tries to extract the parton densities in real photons from $\gamma\gamma$ data taken at e^+e^- colliders. An experiment that allows to tag outgoing electrons both in the forward direction and at small but nonvanishing angles has the opportunity to study these effects in some detail, thereby shedding new light on the interplay between soft and hard QCD.

ACKNOWLEDGMENTS

The work of M.D. was supported in part by the U.S. Department of Energy under Contract No. DE-AC02-76ER00881, by the Wisconsin Research Committee with funds granted by the Wisconsin Alumni Research Foundation, by the Texas National Research Laboratory Commission under Grant No. RGFY93-221, as well as by a grant from the Deutsche Forschungsgemeinschaft under the Heisenberg program.

[1] For a recent review, see M. Drees and R. M. Godbole, Pramana **41**, 83 (1993).
[2] AMY Collaboration, R. Tanaka *et al.*, Phys. Lett. B **277**, 215 (1992).
[3] TOPAZ Collaboration, H. Hayashii *et al.*, Phys. Lett. B **314**, 149 (1993).
[4] ALEPH Collaboration, D. Bukulic *et al.*, Phys. Lett. B **313**, 509 (1993).
[5] H1 Collaboration, T. Ahmed *et al.*, Phys. Lett. B **297**, 205 (1992); I. Abt *et al.*, *ibid.* **314**, 436 (1993).
[6] ZEUS Collaboration, M. Derrick *et al.*, Phys. Lett. B **297**, 404 (1992); DESY Report No. 93-151, 1993 (unpublished).
[7] E. Witten, Nucl. Phys. **B120**, 189 (1977).
[8] M. Drees and K. Grassie, Z. Phys. C **28**, 451 (1985).
[9] H. Abramowicz, K. Charchula, and A. Levy, Phys. Lett. B **269**, 458 (1991).
[10] M. Glück, E. Reya, and A. Vogt, Phys. Rev. D **46**, 1973

(1992).
[11] L. E. Gordon and J. K. Storrow, Z. Phys. C **56**, 307 (1992).
[12] P. Aurenche, P. Chiappetta, M. Fontannaz, J. P. Guillet, and E. Pilon, Z. Phys. C **56**, 589 (1992).
[13] W. A. Bardeen and A. Buras, Phys. Rev. D **20**, 166 (1979); **21**, 2041(E) (1980); D. W. Duke and J. F. Owens, *ibid.* **22**, 2280 (1980); G. Rossi, Phys. Lett. **130B**, 105 (1983); I. Antoniadis and G. Grunberg, Nucl. Phys. **B213**, 445 (1983); M. Fontannaz and E. Pilon, Phys. Rev. D **45**, 382 (1992); M. Glück, E. Reya, and A. Vogt, *ibid.* **45**, 3986 (1992).
[14] M. Drees and R. M. Godbole, Phys. Rev. Lett. **67**, 1189 (1991); Z. Phys. C **59**, 591 (1993).
[15] J. R. Forshaw and J. K. Storrow, Phys. Lett. B **278**, 193 (1992); P. Chen, T. L. Barklow, and M. E. Peskin, Phys. Rev. D **49**, 3209 (1994).
[16] C. F. v. Weizsäcker, Z. Phys. **88**, 612 (1934); E. J. Williams, Phys. Rev. **45**, 729 (1992).
[17] R. Bhattacharya, J. Smith, and G. Grammer Jr., Phys. Rev. D **15**, 3267 (1977).
[18] M. Glück, R. M. Godbole, and E. Reya, Z. Phys. C **38**, 441 (1988); **39**, 590(E) (1988); A. C. Bawa and W. J. Stirling, J. Phys. G **15**, 1339 (1989).
[19] S. Frixione, M. L. Mangano, P. Nason, and G. Ridolfi, Phys. Lett. B **319**, 339 (1993).
[20] T. Uematsu and T. F. Walsh, Nucl. Phys. **B199**, 93 (1982); G. Rossi, Phys. Rev. D **29**, 852 (1984).
[21] F. M. Borzumati and G. A. Schuler, Z. Phys. C **58**, 139 (1993).
[22] S. J. Brodsky, T. Kinoshita, and H. Terazawa, Phys. Rev. D **4**, 1532 (1971); V. M. Budnev, I. F. Ginzburg, G. V. Meledin, and V. G. Serbo, Phys. Rep. **15**, 181 (1974).
[23] G. Bonneau, M. Gourdin, and F. Martin, Nucl. Phys. **B54**, 573 (1973).
[24] J. H. Field, Nucl. Phys. **B168**, 477 (1980).
[25] P. Aurenche, J. P. Guillet, M. Fontannaz, Y. Shimizu, J. Fujimoto, and K. Kato, KEK Report No. 93-180, 1993 (unpublished).
[26] T. Sjöstrand, Phys. Lett. **157B**, 321 (1985); T. Gottschalk, Nucl. Phys. **B277**, 700 (1986).
[27] G. Altarelli and G. Parisi, Nucl. Phys. **B126**, 298 (1977).
[28] W. H. Smith (private communication).
[29] M. Drees and R. M. Godbole, Phys. Rev. D **39**, 169 (1989).